Vol 458|23 April 2009|doi:10.1038/nature07949

LETTERS

Impact of changes in diffuse radiation on the global land carbon sink

Lina M. Mercado[1], Nicolas Bellouin[2], Stephen Sitch[2], Olivier Boucher[2], Chris Huntingford[1], Martin Wild[3] & Peter M. Cox[4]

Plant photosynthesis tends to increase with irradiance. However, recent theoretical and observational studies have demonstrated that photosynthesis is also more efficient under diffuse light conditions[1–5]. Changes in cloud cover or atmospheric aerosol loadings, arising from either volcanic or anthropogenic emissions, alter both the total photosynthetically active radiation reaching the surface and the fraction of this radiation that is diffuse, with uncertain overall effects on global plant productivity and the land carbon sink. Here we estimate the impact of variations in diffuse fraction on the land carbon sink using a global model modified to account for the effects of variations in both direct and diffuse radiation on canopy photosynthesis. We estimate that variations in diffuse fraction, associated largely with the 'global dimming' period[6–8], enhanced the land carbon sink by approximately one-quarter between 1960 and 1999. However, under a climate mitigation scenario for the twenty-first century in which sulphate aerosols decline before atmospheric CO_2 is stabilized, this 'diffuse-radiation' fertilization effect declines rapidly to near zero by the end of the twenty-first century.

The solar radiation reaching the Earth's surface is the primary driver of plant photosynthesis. Leaf photosynthesis increases nonlinearly with incident photosynthetically active radiation (PAR), saturating at light levels that are often exceeded on bright days during the growing season (Fig. 1). Under clear-sky conditions, a fraction of the plant canopy is illuminated by direct solar radiation consisting of bright 'sunflecks', with the remaining portion of the canopy being in the shade. The sunlit fraction of the canopy has leaves that are often light saturated and therefore have low light-use efficiency, whereas leaves in the shade are more light-use efficient but suffer from a lower exposure to incoming radiation. In contrast, under cloudy or aerosol-laden skies, sunlight is more scattered and incoming radiation is more diffuse, producing a more uniform irradiance of the canopy with a smaller fraction of the canopy likely to be light saturated. As a result, canopy photosynthesis tends to be significantly more light-use efficient under diffuse sunlight than under direct sunlight[3]. Hence, the net effect on photosynthesis of radiation changes associated with an increase in clouds or scattering aerosols depends on a balance between the reduction in total PAR (which tends to reduce photosynthesis) and the increase in the diffuse fraction of the PAR (which tends to increase photosynthesis). Although some global climate/carbon-cycle models include the effects of atmospheric aerosols on total irradiance and surface temperature (see, for example, ref. 9), none has accounted for the effects of clouds and aerosols on the land carbon sink through changes in the diffuse fraction of radiation.

To account for the effects of diffuse radiation on canopy photosynthesis, we modified the JULES land-surface scheme used in the Hadley Centre climate models[10]. JULES includes a multilayer approach to scale photosynthesis from the leaf to the canopy. In this study, we also separated each canopy layer into sunlit and shaded regions[11]. Figure 1 shows a comparison of the simulated light response of the gross primary productivity (GPP) with measurements inferred from the eddy correlation technique under direct and diffuse irradiance conditions within a broadleaf temperate forest[12] and a needleleaf temperate forest[13]. The modified JULES

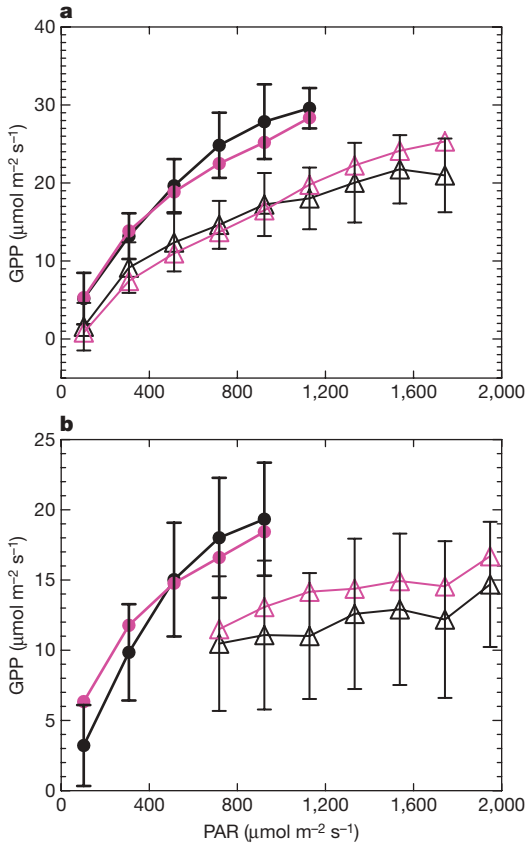

Figure 1 | JULES model evaluation against observations. Observed and modelled light response of the GPP to both direct and diffuse PAR (open triangles and filled circles, respectively) averaged over bins of 200 μmol quanta per square metre per second: **a**, broadleaf forest site; **b**, needleleaf forest site. For the purposes of this validation, data points are split into 'diffuse' and 'direct' conditions, using diffuse fractions of greater than 80% and less than 25% to discriminate between these two cases. Measurements inferred from eddy correlation are given in black (error bars, 1 s.d.), and simulations are given in pink (Methods).

[1]Centre for Ecology and Hydrology, Wallingford OX10 8BB, UK. [2]Met Office Hadley Centre, Exeter EX1 3PB, UK. [3]ETH Zurich, Institute for Atmospheric and Climate Science, CH 8092 Zurich, Switzerland. [4]School of Engineering, Computer Science and Mathematics, University of Exeter, Exeter EX4 4QF, UK.

model can reproduce the different light-response curves under diffuse and direct radiation within the error bars of the observations. A sensitivity analysis carried out for the broadleaf forest shows that the simulated GPP reaches a maximum at a diffuse fraction of 0.4, after which it decreases owing to a reduction in total PAR (Supplementary Fig. 1). The existence of such an optimum is in agreement with a previous modelling study for the same site[14].

We performed multiple global simulations with JULES for the period 1901–2100 to assess the impact of changing diffuse radiation on the global land carbon sink. For 1901–1999, we used an observed monthly climatology of the main climate variables[15], except direct and diffuse total shortwave and PAR fluxes, which were reconstructed using radiative-transfer calculations. The reconstruction takes into account the scattering and absorption of solar radiation by tropospheric aerosols as simulated by the Hadley Centre Global Environmental Model (version HadGEM2-A)[16], a climatology of stratospheric aerosols[17] and a cloudiness data set[15] (Methods). For 2000–2100, we prescribed varying atmospheric CO_2 concentrations and monthly fields of anthropogenic aerosols, following an Intergovernmental Panel on Climate Change SRES A1B scenario modified to stabilise at 450 p.p.m.v of CO_2 equivalent (ENSEMBLES A1B-450)[18]. In this scenario, the diffuse fraction increases during the second half of the twentieth century and then decreases during the twenty-first century owing to correspondingly increasing and decreasing anthropogenic aerosols emissions. The uncertain effects of future changes in climate were not considered, to isolate the diffuse-radiation effect.

Aerosols also have indirect effects on the total PAR through their modification of cloud properties, although these effects are more uncertain[19]. To provide an upper estimate of the impact of the first indirect effect (that of aerosols on cloud albedo) on the land biosphere[20], we assume an absolute reduction in below-cloud PAR equal to the absolute reduction in clear-sky PAR due to aerosols[19]. A 'fixed-diffuse-fraction' control simulation was performed by prescribing the mean diffuse fraction for each grid box and month, based on our reconstruction of the period 1901–1910. The remaining climatological variables in this simulation (including the total PAR) varied as in the first simulation, enabling us to isolate the effect of the varying diffuse fraction as the difference between these two model runs. (See Methods and Supplementary Information for a description of other sensitivity tests performed.)

The eruption of Mount Pinatubo, in the Philippines, in 1991 provided a natural test of the impact of a large increase in stratospheric aerosol loading on the land carbon cycle. The main climatic consequences of the eruption were a cooling of the surface, due to scattering aerosols, and an anomalously low growth rate of the atmospheric CO_2 concentration in both 1992 and 1993, due to an enhanced terrestrial carbon sink[21,22]. Several explanations have been proposed to explain this anomalous land sink, including suppression of plant and heterotrophic respiration during the relatively cool summers[23,24] and enhanced canopy photosynthesis as a result of the post-Pinatubo increase in diffuse fraction[2,3]. However, the relative contributions of these processes during the post-Pinatubo years of 1992 and 1993, and their spatial distribution, remain uncertain.

JULES simulates anomalous land carbon sinks of 1.13 and 1.53 PgC yr^{-1} (petagrams of carbon per year) during 1992 and 1993, respectively, in general agreement with the land flux inferred from observations[22,25] (Fig. 2). Our model suggests a major contribution of diffuse radiation to the land sink anomaly in 1992 of 1.18 PgC yr^{-1}, but a much smaller contribution in 1993 of 0.04 PgC yr^{-1} (red wedge, Fig. 2a). Carbon sink anomalies of 1.05 PgC yr^{-1} and 0.92 PgC yr^{-1} are associated with the anomalously cool air temperatures in 1992 and 1993 (anomalies of −0.33 K and −0.21 K), which act to suppress heterotrophic respiration (for further details, see Supplementary Figs 2–5).

A decrease in total solar radiation[6–8], termed global dimming, was observed at the Earth's surface during the 1950–1980 period. This decrease is consistent with the impacts of anthropogenic aerosols on cloud properties, water vapour and cloud feedbacks due to global warming[26]. Increases in cloud thickness, cloud cover and scattering aerosols enhance the diffuse component of the radiation reaching the surface, whereas increasing concentrations of absorbing aerosols can have the opposite effect[27]. As a result, observed trends in diffuse radiation are not as coherent as those in total radiation during the dimming period[28–30]. Since the 1980s, industrialised regions of the Northern Hemisphere appear to have 'brightened'[8]. This has been associated with reduced anthropogenic emissions of aerosol precursors (especially sulphur dioxide) in these regions.

Figure 3a shows changes in the diffuse fraction of the PAR as reconstructed using cloud cover[15] and aerosol distributions. The simulated total shortwave radiation and diffuse fraction compare well with ground-based radiation measurements (Supplementary Figs 6 and 7). The contribution of variations in diffuse fraction to the simulated land carbon sink becomes important after 1950 (Fig. 3b). This contribution increases during the global dimming period (1960–1980), when it adds 0.44 PgC yr^{-1} to the mean land carbon sink, and lessens during the subsequent brightening period

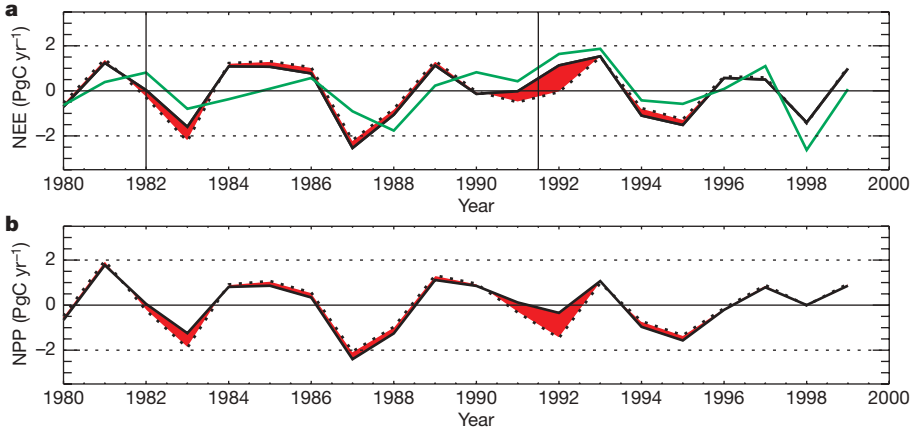

Figure 2 | Net ecosystem exchange (NEE) and net primary productivity (NPP). a, Inferred NEE values (derived from atmospheric CO_2 measurements[21] and simulated ocean flux[25]) are shown by the green line. Also presented are simulated global detrended flux anomalies of NEE (black) under varying (continuous line) and fixed (dashed line) diffuse fraction. The red shaded area corresponds to the contribution of the varying diffuse fraction to simulated NEE, calculated as the difference between the fluxes simulated under conditions of varying and fixed diffuse fraction. NEE is defined as the difference between net primary productivity (NPP) and heterotrophic respiration. Vertical lines correspond to the timing of the El Chichón (Mexico) and Pinatubo volcanic eruptions, respectively. **b**, Simulated NPP values for varying (continuous line) and fixed (dashed line) diffuse fraction, with the red shaded area again corresponding to the contribution of varying diffuse irradiance to simulated NPP.

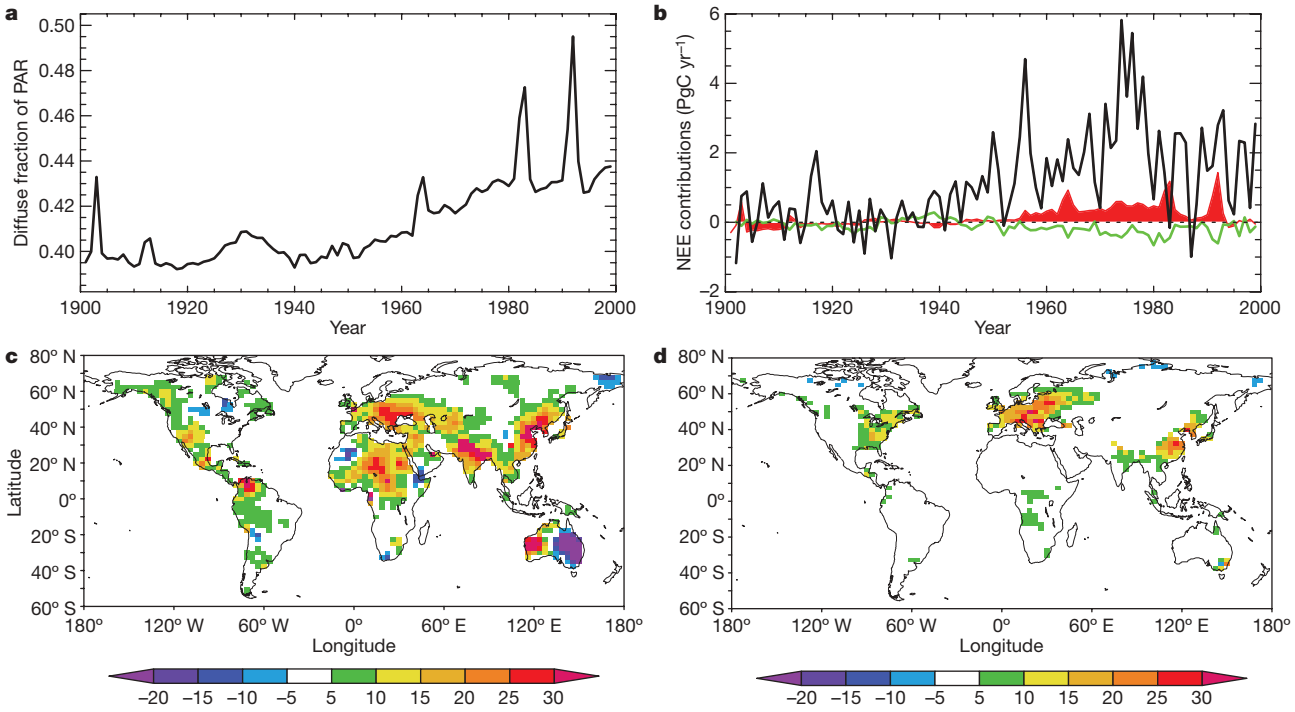

Figure 3 | Impact of changes in diffuse fraction on the land carbon sink during the twentieth century. **a**, Simulated global mean annual diffuse fraction of the PAR, based on aerosol optical depth from volcanic[17] and anthropogenic sources, as simulated by HadGEM2-A, and observed Climate Research Unit cloudiness[15]. **b**, Simulated contribution of diffuse fraction to simulated land NEE (red), calculated as the difference between simulated NEE under varying diffuse fraction (black, total NEE) minus simulated NEE under constant diffuse fraction (not shown) and simulated contribution of the total PAR to simulated land NEE (green). **c**, Simulated percentage change (colour scale) in diffuse fraction between 1950 and 1980. **d**, Simulated change (colour scale, grams carbon per square metre per year) in diffuse-fraction contribution to land carbon accumulation between 1950 and 1980.

(1980–1999), when it contributes a mean of 0.3 PgC yr^{-1}, as a result of decreasing diffuse fraction.

The HadGEM2-A reconstruction suggests geographically varying changes in diffuse fraction of −20% to 30% between 1950 and 1980 (Fig. 3c). The corresponding impact on the regional land sink is estimated to be large, reaching up to 30 gC m^{-2} yr^{-1} across Europe, the eastern United States, East Asia and some tropical regions in Africa (Fig. 3d). By contrast, during the brightening period 1980–1999 (Supplementary Fig. 8), the HadGEM2-A reconstruction suggests a reduction in diffuse fraction over Europe, the eastern United States, Western Australia and some regions of Russia and China, leading to a reduction in the regional contribution of the diffuse fraction to the total land carbon accumulation during this period. Overall, these results suggest that increases in diffuse fraction have enhanced the global land carbon sink by 23.7% between 1960 and 1999 (Fig. 4b). As shown in Supplementary Fig. 9, the contributions of diffuse fraction to the land sink are of similar magnitude to the net contributions of variations in temperature and precipitation during this period.

Neglecting diffuse-radiation fertilization, as in the current generation of global models, we estimate that reductions in total PAR would have caused a −14.4% change in the mean land carbon sink. Instead, we model a net enhancement of the land carbon sink by overall (diffuse and direct) radiation changes of +9.3%, as diffuse-radiation fertilization overwhelms global dimming (see Supplementary Fig. 10 for regional contributions to the GPP). Contrary to the results of current global models, it therefore seems that anthropogenic aerosols have enhanced land carbon uptake during this period, despite significant reductions in total PAR. Fully coupled Earth-system-model simulations are now required to confirm this result when accounting for the effects of short-timescale variability in atmospheric aerosol loading.

To project these results into the twenty-first century, the environmentally friendly emissions scenario mentioned above (ENSEMBLES

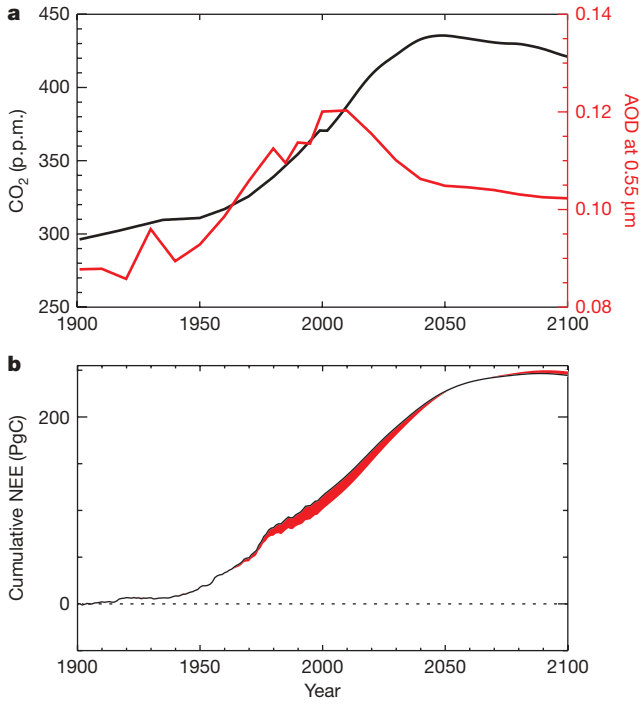

Figure 4 | Historical and twenty-first-century projections (according to the ENSEMBLES A1B-450 stabilization scenario). **a**, Prescribed atmospheric CO_2 (black) and aerosol optical depth (red). **b**, Simulated contribution of diffuse-fraction variations (red) to the cumulative land carbon sink (black) during the 1900–2100 period. In this scenario, future climate change for the twenty-first century was not considered, and climate variables, including cloud cover, were taken to be fixed at their 1999 values throughout the simulation of the twenty-first century.

A1B-450) was assumed, in which total greenhouse gas concentrations stabilize at 450 p.p.m.v. CO_2 equivalent and sulphate and black-carbon aerosol emissions decline rapidly. In this scenario, atmospheric CO_2 peaks at 435 p.p.m.v. around 2050 before declining steadily to reach 421 p.p.m.v. by 2100. The total aerosol optical depth (AOD) declines steeply from its 2000 maximum of 0.12 and levels off at 0.10 by 2050 (Fig. 4a). As a result, the HadGEM2-A reconstruction suggests a rapid reduction in the diffuse fraction of the PAR, which leads to a rapid decline in the contribution of diffuse radiation to the land carbon sink. By 2100, diffuse-radiation fertilization is lost (Fig. 4b). We conclude that steeper cuts in fossil-fuel emissions will be required to stabilize the climate if anthropogenic aerosols decline as expected.

METHODS SUMMARY

This study uses the JULES land-surface scheme[10], which takes into account variations in direct and diffuse radiation on sunlit and shaded canopy photosynthesis. We added a description of sunfleck penetration through the canopy[11] and separated each layer of the canopy into sunlit and shaded regions. In this way, photosynthesis of sunlit and shaded leaves was calculated separately under the assumption that shaded leaves receive only diffuse light and sunlit leaves receive both diffuse and direct radiation.

We obtained the geographical distributions of the downward direct and diffuse radiative fluxes throughout the twentieth and twenty-first centuries by coupling distributions of clouds and aerosols (tropospheric and stratospheric[17]) using look-up tables of radiative-transfer calculations. Distributions of AOD at 0.55 μm for six tropospheric aerosol species for the twentieth century were taken from simulations of HadGEM2-A, the atmospheric version of the latest Hadley Centre Global Environmental Model. AOD distributions for sulphate and black carbon in the twenty-first century were obtained by scaling the distributions for the year 2000 according to changes in ammonium sulphate burden obtained using the ENSEMBLES A1B-450 scenario relying on the A1B storyline and the methodology from ref. 18. We left the four other tropospheric aerosol species, and stratospheric aerosols, unchanged at their 2000 levels because their future evolutions are uncertain.

This study uses the 0.5° resolution observed monthly climatology from ref. 15. All monthly data were regridded onto a 2.5° × 3.75° grid and disaggregated to hourly data. We did not consider future climate change for the twenty-first century, and climate variables, including cloud cover, were taken as fixed at their year 1999 values throughout the simulation of the twenty-first century.

Percentage changes in the land carbon sink were calculated relative to our fixed-diffuse-fraction control simulation.

Full Methods and any associated references are available in the online version of the paper at www.nature.com/nature.

Received 5 September 2008; accepted 24 February 2009.

1. Goudriaan, J. *Crop Micrometeorology: A Simulation Study* 5–72 (Centre for Agricultural Publishing and Documentation, 1977).
2. Gu, L. H. *et al.* Response of a deciduous forest to the Mount Pinatubo eruption: enhanced photosynthesis. *Science* **299,** 2035–2038 (2003).
3. Roderick, M. L., Farquhar, G. D., Berry, S. L. & Noble, I. R. On the direct effect of clouds and atmospheric particles on the productivity and structure of vegetation. *Oecologia* **129,** 21–30 (2001).
4. Niyogi, D. *et al.* Direct observations of the effects of aerosol loading on net ecosystem CO_2 exchanges over different landscapes. *Geophys. Res. Lett.* **31,** doi:10.1029/2004GL020915 (2004).
5. Oliveira, P. H. F. *et al.* The effects of biomass burning aerosols and clouds on the CO_2 flux in Amazonia. *Tellus B* **59,** 338–349 (2007).
6. Stanhill, G. & Cohen, S. Global dimming: a review of the evidence for a widespread and significant reduction in global radiation with discussion of its probable causes and possible agricultural consequences. *Agric. For. Meteorol.* **107,** 255–278 (2001).
7. Liepert, B. G. Observed reductions of surface solar radiation at sites in the United States and worldwide from 1961 to 1990. *Geophys. Res. Lett.* **29,** doi:10.1029/2002GL014910 (2002).
8. Wild, M. *et al.* From dimming to brightening: decadal changes in solar radiation at Earth's surface. *Science* **308,** 847–850 (2005).
9. Jones, C. D., Cox, P. M., Essery, R. L. H., Roberts, D. L. & Woodage, M. J. Strong carbon cycle feedbacks in a climate model with interactive CO_2 and sulphate aerosols. *Geophys. Res. Lett.* **30,** doi:10.1029/2003GL016867 (2003).
10. Mercado, L. M., Huntingford, C., Gash, J. H. C., Cox, P. M. & Jogireddy, V. Improving the representation of radiation interception and photosynthesis for climate model applications. *Tellus B* **59,** 553–565 (2007).
11. Dai, Y. J., Dickinson, R. E. & Wang, Y. P. A two-big-leaf model for canopy temperature, photosynthesis, and stomatal conductance. *J. Clim.* **17,** 2281–2299 (2004).
12. Knohl, A., Schulze, E. D., Kolle, O. & Buchmann, N. Large carbon uptake by an unmanaged 250-year-old deciduous forest in central Germany. *Agric. For. Meteorol.* **118,** 151–167 (2003).
13. Rebmann, C. *et al.* Influence of transport processes on CO_2-exchange at a complex forest site in Thuringia, Germany. *Agric. For. Meteorol.* (submitted).
14. Knohl, A. & Baldocchi, D. D. Effects of diffuse radiation on canopy gas exchange processes in a forest ecosystem. *J. Geophys. Res.* **113,** doi:10.1029/2007JG000663 (2008).
15. New, M., Hulme, M. & Jones, P. Representing twentieth-century space-time climate variability. Part II: Development of 1901–96 monthly grids of terrestrial surface climate. *J. Clim.* **13,** 2217–2238 (2000).
16. Bellouin, N. *Improved Representation of Aerosols for HadGEM2.* Technical Note 73, ⟨http://www.metoffice.gov.uk/publications/HCTN/HCTN_73.pdf⟩ (Met Office Hadley Centre, 2007).
17. Sato, M., Hansen, J., McCormick, M. & Pollack, J. Stratospheric aerosol optical depths, 1850–1990. *J. Geophys. Res.* **98,** 22987–22994 (1993).
18. van Vuuren, D. P. *et al.* Stabilizing greenhouse gas concentrations at low levels: an assessment of reduction strategies and costs. *Clim. Change* **81,** 119–159 (2007).
19. Forster, P. *et al.* in *Climate Change 2007: The Physical Science Basis* (eds Solomon, S. *et al.*) 129–234 (Cambridge Univ. Press, 2007).
20. Gu, L., Fuentes, J. D., Shugart, H. H., Staebler, R. M. & Black, T. A. Responses of net ecosystem exchanges of carbon dioxide to changes in cloudiness: results from two North American deciduous forests. *J. Geophys. Res.* **104,** 31421–31434 (1999).
21. Ciais, P., Tans, P. P., Trolier, M., White, J. W. C. & Francey, R. J. A large northern-hemisphere terrestrial CO_2 sink indicated by the C-13/C-12 ratio of atmospheric CO_2. *Science* **269,** 1098–1102 (1995).
22. Keeling, C. D., Whorf, T. P., Wahlen, M. & Vanderplicht, J. Interannual extremes in the rate of rise of atmospheric carbon-dioxide since 1980. *Nature* **375,** 666–670 (1995).
23. Lucht, W. *et al.* Climatic control of the high-latitude vegetation greening trend and Pinatubo effect. *Science* **296,** 1687–1689 (2002).
24. Jones, C. D. & Cox, P. M. Modeling the volcanic signal in the atmospheric CO_2 record. *Glob. Biogeochem. Cycles* **15,** 453–465 (2001).
25. Buitenhuis, E. *et al.* Biogeochemical fluxes through mesozooplankton. *Glob. Biogeochem. Cycles* **20,** doi:10.1029/2005GB002511 (2006).
26. Romanou, A. *et al.* 20th century changes in surface solar irradiance in simulations and observations. *Geophys. Res. Lett.* **34,** doi:10.1029/2006GL028356 (2007).
27. Liepert, B. & Tegen, I. Multidecadal solar radiation trends in the United States and Germany and direct tropospheric aerosol forcing. *J. Geophys. Res.* **107,** doi:10.1029/2001JD000760 (2002).
28. Power, H. C. Trends in solar radiation over Germany and an assessment of the role of aerosols and sunshine duration. *Theor. Appl. Climatol.* **75,** 47–63 (2003).
29. Russak, V. Changes in solar radiation and their influence on temperature trend in Estonia (1955–2007). *J. Geophys. Res.* **114,** doi:10.1029/2008JD010613 (2009).
30. Long, C. N., Dutton, E. G., Augustine, J. A., Wiscombe, W. & Wild, M. Investigations of surface downwelling solar radiation for the continental US. *J. Geophys. Res.* (in the press).

Supplementary Information is linked to the online version of the paper at www.nature.com/nature.

Acknowledgements We thank A. Knohl and C. Rebmann for supplying the eddy flux data for model evaluation, D. van Vuuren and the group that developed the IMAGE model for providing scenario data for the simulation of the twenty-first century. We also thank C. D. Jones for advice on the experimental design, C. M. Taylor for discussions on early results, R. Ellis and P. Harris for both scientific and technical support, A. Everitt for computer support and G. Weedon for discussions. The authors acknowledge funding from the UK Natural Environment Research Council CLASSIC programme (L.M.M., C.H. and P.M.C.) and the UK Department for Environment, Food and Rural Affairs (Defra) and the UK Ministry of Defence (MoD) (N.B., O.B. and S.S.) under GA01101 (Defra) and CBC/2B/0417_Annex C5 (MoD) and from the Swiss NCCR Climate (M.W.).

Author Contributions L.M.M. and P.M.C. developed the modification of the JULES model to include sunfleck penetration through the canopy. L.M.M. validated the model at site level, analysed and performed the global simulations and wrote the initial version of the manuscript. O.B. and N.B. developed the framework for producing the shortwave and PAR fields. N.B. developed the look-up tables to reconstruct shortwave and PAR fields under clear- and cloudy-sky conditions and validated the output against ground-based observations. O.B. provided the sulphate aerosol burden for the simulation of the twenty-first century. P.M.C. contributed to the entire study and S.S. contributed to the analysis of results. C.H. developed the IMOGEN software that enabled the global simulations to be carried out. M.W. provided ground-based observations of shortwave- and diffuse-radiation time series and also advised on model validation. All authors discussed the results and the structure of the paper and developed and improved the manuscript.

Author Information Reprints and permissions information is available at www.nature.com/reprints. Correspondence and requests for materials should be addressed to L.M.M. (lmme@ceh.ac.uk).

METHODS

Shortwave and PAR fields. Geographical distributions of the downward direct and diffuse radiative fluxes throughout the twentieth and twenty-first centuries were obtained using look-up tables of radiative-transfer calculations driven by distributions of clouds and aerosols. Aerosol distributions were simulated using the atmospheric component of the Hadley Centre Global Environmental Model version 2 (HadGEM2-A)[16], which includes six tropospheric aerosol species (sulphate, black carbon, mineral dust, sea salt and biomass burning). Model evaluation against ground-based Sun-photometer measurements shows model underestimation of AOD over Europe and North America in winter and northwestern Africa during mineral-dust and biomass-burning events. However, simulations are good during summer and throughout the year in Asia, southern Africa, and South America[16].

Changes in AOD throughout the twentieth century were obtained by varying emissions of aerosols and their precursors. Distributions of tropospheric aerosol optical depths for the six aerosol species were provided at a resolution of 1.25° latitude by 1.875° longitude as monthly means every ten years between 1900 and 1980, and every five years between 1980 and 2000. Monthly distributions for the years between were linearly interpolated from the modelled distributions. Distributions of stratospheric aerosols from the twentieth century were taken as zonal means from ref. 17.

AOD distributions for sulphate and black carbon in the twenty-first century were obtained by scaling the distributions for the year 2000 according to changes in the ammonium sulphate burden simulated by a chemistry–climate model using the ENSEMBLES A1B-450 scenario relying on the A1B storyline and the methodology from ref. 18. The four other tropospheric aerosol species, and stratospheric aerosols, were left unchanged at their 2000 levels, as their future evolution is uncertain.

Radiative-transfer calculations. Downward direct and diffuse radiative fluxes were obtained independently for the clear-sky (cloud-free) and cloudy part of each grid box. These fluxes were pre-computed and stored in look-up tables for the shortwave (0.28–4.0-μm) and PAR (0.40–0.69-μm) spectra.

Under clear-sky conditions, downward direct and diffuse radiative fluxes depend on the solar zenith angle, the type and optical depth of the tropospheric aerosol and the optical depth of the stratospheric aerosol. Aerosol phase function and scattering and absorption coefficients were computed for all aerosol species at 24 wavelengths using Mie calculations. The computed aerosol optical properties were used in a discrete-ordinate solver[31] to obtain radiative fluxes. Tropospheric aerosols were assumed to be homogeneously distributed across the lowest kilometre of the atmosphere; stratospheric aerosols reside in a homogeneous layer between 15 and 20 km above ground.

Under cloudy-sky conditions, the cloud type and optical thickness were not given by the Climate Research Unit (CRU) data set[15]. The only characterization of clouds in the CRU data set is their fractional cover, which contains little information useful in determining downward shortwave and PAR fluxes. To circumvent this issue, quadratic relationships between cloud cover and atmospheric transmission were derived from simulations using HadGEM2-A over each continent, on a monthly basis. Here the atmospheric transmission is the ratio between the downward shortwave flux at the surface and the incoming shortwave flux at the top of the atmosphere. Using this ratio, the diurnal cycle of incoming shortwave flux was imposed on the downward flux at the surface. These relationships thus provided a means of reproducing the monthly averaged downward flux simulated by the climate model but using the observed CRU cloud-cover data set as an input. The downward flux in the cloudy fraction of a grid box was assumed to be purely diffuse, which is a good approximation except at very low cloud optical depth. Fluxes in the PAR spectral bands were obtained by assuming that cloud extinction was constant throughout the shortwave spectrum. Under this assumption, PAR fluxes are 41% of shortwave fluxes. A comparison of simulated total shortwave flux and diffuse fraction with ground-based observations (Supplementary Figs 6 and 7) allowed us to adjust the cloudy-sky flux look-up table, with a reduction of 25% of the fluxes to retain the set of parameters that fit best the observed fluxes.

The clear-sky flux in a given grid box at a given time and date was obtained from the look-up table record corresponding to the current solar zenith angle, and tropospheric and stratospheric aerosol optical depths. As the look-up tables did not include combinations of different tropospheric aerosol types, the whole tropospheric column was assumed to have the optical properties of the dominant aerosol. Look-up table fluxes were linearly interpolated in solar zenith angle and tropospheric aerosol optical depth. The reconstructed clear-sky surface fluxes compared very well with those computed using HadGEM2-A. The cloudy-sky flux was derived from the value of the cloud cover in the grid box, and the solar zenith angle determined the incoming solar radiation. Finally, cloudy- and clear-sky fluxes were weighted by the cloud cover and the clear-sky fractions, respectively, to obtain the grid-box-averaged downward direct and diffuse fluxes in the shortwave and PAR spectra.

JULES evaluation at single sites. Evaluation of JULES was carried out using hourly values of eddy correlation flux data and meteorology from two German sites, a temperate broadleaf forest site (Hainich)[12] and a temperate needleleaf forest site (Wetzstein)[13], during the summer. Meteorological forcing and diffuse radiation measured in parallel with the eddy correlation fluxes were used to force the model. To evaluate the global model at individual flux sites, we calibrated model parameters to fit local ecological conditions. In particular, the model parameter that represents the maximum photosynthetic capacity, V_{max}, was set at 60 and 40 μmol m^{-2} s^{-1} for the broadleaf and needleleaf sites, respectively. The corresponding values used in the global model were 32 and 24 μmol m^{-2} s^{-1}.

Vegetation cover was updated using the TRIFFID dynamic global vegetation model, which includes a rudimentary model of leaf phenology based on growing degree days. Changes in land use were neglected; instead, a fixed land-use mask was prescribed to account for present-day crop and pasture lands.

31. Key, J. R. & Schweiger, A. J. Tools for atmospheric radiative transfer: Streamer and FluxNet. *Comput. Geosci.* **24**, 443–451 (1998).